Effect of calcium addition on Mg-AlOx supported Ni catalysts for hydrogen production from pyrolysis-gasification of biomass

Fangzhu Jin[a], Hongman Sun[b], Chunfei Wu[b*], Huajuan Ling[a], Yijiao Jiang[c], Paul T. Williams[d*], Jun Huang[a*]

[a] School of Chemical and Bimolecular Engineering, the University of Sydney, Australia, NSW 2037
(Tel: +61 2 9351 7483; Email: jun.huang@sydney.edu.au)
[b] School of Engineering and Computer Science, University of Hull, Hull, HU6 7RX
(Tel: +44 1482 466464; Email:C.Wu@hull.ac.uk)
[c] Department of Engineering, Macquarie University, Sydney, New South Wales 2109, Australia
[d] School of Chemical & Process forEngineering, University of Leeds, Leeds LS2 9JT, UK
(Tel: +44 113 3432504; Email: p.t.williams@leeds.ac.uk)

Abstract: Producing hydrogen from catalytic gasification of biomass represents an interesting process to facilitate the development of hydrogen economy. However, the design of catalyst is a key challenge for this technology. In this work, cost-effective Ca added Ni-based catalysts were developed and studied for producing hydrogen with a fixed-bed reactor. The relationship between Ca addition and the performance of catalyst in terms of the yield of hydrogen and catalyst deactivation (metal sintering and coke formation) was studied. The results showed that hydrogen production was largely enhanced when Ca was added, as the yield of hydrogen was enhanced from 10.4 to 18.2 mmol g^{-1} sample in the presence of Ca-based catalyst. However, the yield and concentration of hydrogen were kept at similar levels with the increase of Ca. By normalizing the yield of hydrogen in relation to the amount of Ni presented inside the catalyst, the hydrogen yield per mole of nickel was increased from 50 g Ni $^{-1}$(0.1Ca catalyst) to 80g Ni^{-1} (0.8Ca catalyst) when the Ca addition was increased from 10 mol.% to 80 mol.%. TPO-FTIR analysis of the experimented catalysts showed that 0.5 Ca catalyst had the highest amount of coke formation, in particular, most of the deposited carbons were amorphous which could deactivate the catalyst seriously. It is therefore concluded that the addition of cost-effective Ca could enhance the yield of hydrogen from biomass gasification. However, the concentration of Ca in the catalyst needs to be controlled to mitigate the generation of coke on the used catalyst.

Key words: Biomass; Gasification; Ca promoted Ni catalysts; Reforming; Hydrogen

1. Introduction

Hydrogen represents a promising energy carrier that can be widely used for power generation and chemical production [1]. It can be produced from a verity of sources. Among them, biomass is considered to be an approximately carbon neutral resource and a promising raw material to generate hydrogen through gasification process. However, compared to the processing of fossil fuels, gasification of biomass still suffers from lower hydrogen production. Therefore, catalysts are commonly utilized to improve the yield of hydrogen from biomass. Even though noble metal catalysts including Pt and Rh etc. are efficient to improving the hydrogen production, the expensive cost limits the practical applications [2, 3]. Transition metals especially nickel catalysts have attracted much attention for producing hydrogen from biomass gasification due to the relative low cost of metals and high redox activity [4-6]. However, sintering and coke deposition can cause catalyst deactivation; this is a significant problem for practical catalyst applications [7, 8]. Therefore, several strategies such as controlling support properties [9-11] and using bimetallic metals [12-14] have been developed to reduce metal sintering and improve the performance of nickel catalysts.

The addition of basic alkali earth metals into Ni-based catalysts attracted intensive attention in inhibiting coke deposition and improving the catalytic activity due to the promotion of carbon oxidation. The addition of CaO to Ni-based catalyst has been identified as an effective approach to improve methane conversion and catalyst stability in methane reforming process [15-17]. Hou et al. [18] studied the effect of Ca on a supported nickel catalyst for methane dry reforming. The results indicated that the presence of Ca increased the conversion of methane and the stability of the $Ni/r-Al_2O_3$ due to Ca could improve Ni dispersion, strengthening the interaction between support and Ni particles. In addition, Kariny et al. [19] modified Ni/Al_2O_3 catalysts using CaO (0-5 wt %) to enhance ethanol conversion for hydrogen production. The 5Ni-5Ca/Al catalyst exhibited the lowest coke deposition ($0.01 molg^{-1}$) for the reforming reaction and no deactivation was found after 24 h in the stability test. They proposed that the introduction of CaO into the Ni/Al_2O_3 catalyst led to structure changes, leading to a stronger integration between metal and support. Therefore, a lower activation temperature was required for ethanol reforming reactions. Catherine et al. [20] also studied Ca-containing Ni/Al_2O_3 catalyst with different Ca contents. It was reported that Ca addition could increase Ni particle size from 6.0 nm to 9.0 nm, which resulted in the formation of encapsulating carbons. In addition, the $10Ni/3Ca-Al_2O_3$ demonstrated excellent catalytic performance and superior stability for at least

24 h due to effective coke removal. Ca loading was reported to significantly reduce coke formation on the reacted catalyst, because the particle size of Ni, the valence band of catalyst and the rate of steam coke reaction were influenced by the loading of Ca. Moreover, Sengupta et al. [11] modified catalyst support with CaO and MgO to improve the catalytic activity of Al_2O_3 supported with Ni and Ni-Co for methane dry reforming. The authors reported that the presence of CaO had a favorable effect on methane conversion, which was attributed to the interaction between CaO and Ni species. However, MgO had an adverse effect on the conversion of methane as ascribed to a strong interaction between MgO and Ni and Co phases was formed.

It was also reported that CaO acting as CO_2 absorbent could promote water-gas shift reaction to increase the production of hydrogen from gasification [21, 22]. In addition, high CO_2 adsorption capacity can accelerate the activation of CO_2 and decrease carbon deposition on the reacted catalyst [16, 23, 24]. Therefore, it seems that the addition of Ca into Ni-catalyst system is promising to increase the yield of hydrogen and to reduce the deposition of coke on reacted catalyst. However, there is no systematic investigation about the addition of Ca on producing hydrogen from biomass gasification. In this study, cost-effective Ca was added to Ni-catalysts for improving hydrogen production using a fixed-bed two-stage reactor. The relationship between Ca addition and the catalytic activities for producing hydrogen and the coke formation and metal sintering on the reacted catalysts was studied.

2. Experimental

2.1 Raw biomass sample and catalyst materials

Wood sawdust (less than 0.2 mm particle size) was selected as raw feedstock for this work. The biomass sample has 5.7 wt.% moisture, 18.3 wt.% fixed carbon, 74.8 wt.% volatile, and 1.2 wt.% ash. In addition, the sample has 47.1 wt.% C, 5.9 wt.% H, 46.9 wt.% O and 0.1 wt.% N.

Ca-Ni-Mg-Al (1:2:2:1 mole ratio), Ni-Mg-Al (2:2:1 mole ratio), Ni-Ca-Al (2:1:1 mole ratio), Ni-Mg-Al (1:1:1) catalysts with four Ca loadings (0.1%, 0.3 %, 0.5%, 0.8 mole%) were obtained using a co-precipitation method. Initially, the required amounts of $Ca(NO_3)_2 \cdot 4H_2O$, $Ni(NO_3)_3 \cdot 6H_2O$, $Mg(NO_3)_2 \cdot 6H_2O$ and $Al(NO_3)_3 \cdot 9H_2O$ were first dissolved in water, and then Na_2CO_3 solution was added into the precursor solution under continuous stirring with the pH of 8.0. The precursors were washed with water, then were dried at 80°C overnight. The obtained products were calcined in a muffle furnace at 800°C for 4 h in the presence of static air.

2.2 Biomass gasification experiment

Biomass gasification was tested using the prepared Ca added Ni-catalysts using a fixed bed reactor which consisted of two stages. The raw sample was initially decomposed at the first stage. The produced vapors were catalytic reformed/cracked at the second stage. A schematic diagram of the reaction system is shown in a previous work [25]. For the experiment, 1.0 sawdust and around 0.5 g catalyst were used in the first stage and the second reactor, respectively. Prior to the heating of the reactors, N_2 was introduced into the reactor with a flow rate of 80 ml min^{-1}. The second stage where the catalyst was placed was heated to 800 °C, then the first stage where the wood sawdust was placed was heated to 550 °C at a 40 °C min^{-1}. Steam was formed by injecting water into the second stage. The water injection rate was 4.74 g h^{-1}. The outlet of the second stage was connected to a condensation system which was cooled by air and dry-ice, respectively. The gas sample was collected by a gas bag for further analysis. For each experiment, a total reaction time around 40 min was used. Good mass balance of the experiment was obtained to have a good accuracy of experimental data.

2.3 Gas analysis and characterizations of catalysts

A gas chromatography (GC) was applied to determine the concentrations of the produced gases. CO_2 gas concentration was analyzed using a Varian 3380 GC where a Hysep 80-100 mesh column and argon carrier gas were used. Another Varian 3380 GC was used to determine CO, H_2, and N_2 gases when argon was used as carrier gas; the GC had a 60-80 mesh molecular sieve column. C_1-C_4 based gases were analyzed by another Varian 3380 GC with a flame ionization detector while N_2 is working as carrier gas.

Textural properties of the fresh catalysts were analyzed by N_2 adsorption and desorption (Quantachrome Autosorb). Before surface analysis, catalyst sample was degassed at 423K under vacuum for 12 hours.

The crystal phases of the prepared catalysts were obtained using X-ray diffraction (XRD) (SIEMENS D6000) with a scanning range of 1.5-70° using CuKα radiation with a 0.1542 nm wavelength. The morphologies of the fresh and reacted catalyst were obtained by using a scanning electron microscope (SEM) (LEO 1530). In addition, high-resolution images of the catalysts were obtained by using a transmission electron microscopy (TEM) (Philips CM200).

TPO (Temperature-programmed oxidation) was carried out to investigate the information of coke deposited on the surface of the reacted catalysts using a Stanton-Redcroft thermogravimetric analyser (TGA). The produced gases from TPO analysis was analyzed with a Fourier transform infrared spectrometer (FTIR) (Nicolet Magna IR-560) to obtain the yield of CO_2 produced from the oxidation of coke. A Nicolet Magna IR-560 thermogravimetric analyzer connected with a ThermoStar GSD301 mass spectrometer was used to test the reducibility of the fresh catalyst. During the TPR analysis, the sample was initially heated to 500 °C at a heating rate of 20 °C min^{-1} with N_2 carrier gas (500 ml min^{-1}). The sample was then cooled to room temperature before the introduction of H_2. Then TPR was carried out between room temperature and 1000 °C. The heating rate was 10 °C min^{-1}.

3. Results and discussions

3.1. Characterizations of the fresh Ni-Ca-Mg-Al

3.1.1. N_2 adsorption/desorption results of fresh catalysts

BET surface area of the prepared catalyst was shown in Table 1. The BET surface area of the Ca-Ni-Mg-Al (1:2:2:1), the Ni-Mg-Al (2:2:1), the Ca-Ni-Al (1:2:1) was 79.48, 126.29 and 96.54 m^{2}g^{-1}, respectively. With the increase of Ca loading from 0.1 Ca to 0.8 Ca (corresponding to 10 to 80 mol. % of total metals in the catalyst), the surface area was decreased from 153.27 to 98.88 m^{2}g^{-1}, and the particle size was increased from 19.85 to 27.52 nm, as shown in Table 1.

3.1.2. XRD results of the prepared catalysts

The strong peaks at 38º, 43ºand 64º (Figure 1 and Figure 2) were suggested to be the reduction of NiO (101), NiO (012) and NiO (110), respectively. From Figure 1, only the Ca-Ni-Al (1:2:1) sample exhibited two diffraction peaks at 19º and 35º, indicating the presence of $NiAl_2O_4$ [26, 27]. In addition, CaO phase was observed except for the Ni-Mg-Al (2:2:1) catalyst. With the increase of calcium loading, the peak intensity correspond to CaO phase was increased. It is difficult to distinguish $MgAl_2O_4$ from $NiAl_2O_4$, as their diffraction peaks were overlapped in the XRD patterns. As reported, $MgAl_2O_4$ has diffraction peaks at 19.2º, 31.6º, 37.3º, 45.3º, 56.4º, 60.0º and 66.2º (JCPDS 00001-1157) [28]. $NiAl_2O_4$ has diffraction peaks at 19.1º, 31.45º, 37.0º, 45.0º, 59.7º and 65.5º (JCPDS 00-010-0339). NiO has peaks at 37.4º, 43.4º and 63.5º. (JCPDS01-073-1519) [29, 30].

Volume average NiO particle sizes was calculated by Debye-Scherrer equation for the fresh catalyst as shown in Table 1. The crystallite size of NiO particle for the Ca-Ni-Mg-Al catalyst is around 17.98 nm. If there is no Ca loading in the fresh catalyst, the size of NiO particle decreased from 17.98 to 8.8 nm. However, the NiO particle size exhibited slight changes without the addition of Mg in the fresh catalyst.

3.1.2. SEM and TPR results of the prepared catalysts

The morphology of the prepared catalysts was studied by SEM analysis. From Figure 3, the metal distribution is uniform for all the catalysts. However, there was no obvious morphological difference between the fresh catalysts with different Ca loadings.

Figure 4 shows the changes of weight of the prepared catalysts obtained from TPR. The reduction at about 390 °C was suggested to the reduction of bulk NiO presented in the catalyst [31, 32]. The second reduction peak at around 600 °C is suggested to the presence of small NiO particles [18, 33]. The third reduction peak was suggested to be due to the reduction of $NiAl_2O_4$ [34, 35]. The molar fraction of the mentioned Ni-based phases are calculated based on TPR analysis as shown in Table 2.

The 0.1Ca catalyst showed the highest fraction of $NiAl_2O_4$ phase and the lowest fraction of NiO particles. The 0.8Ca catalyst demonstrated the highest percentage of bulk NiO. It is indicated that the ratio of bulk NiO phase was increased when Ca content was increased. The 0.5Ca catalyst showed the highest fraction of small NiO particles.

3.2. Mass balance of experimental studies

The mass balance of pyrolysis/gasification of biomass is shown in Table 3 and Table 4. The mass balance of each experiment was obtained by the total weight of the outputs of the experiment (including gas, liquid in condensers, and char residue) divided by the initial inputs (including biomass feedstock and injected water). A good mass balance (92%~99%) for all the experiments was obtained. Compared to the blank experiment using sand, hydrogen production was significantly increased with the addition of catalyst regardless of the amount of calcium addition. The concentration of hydrocarbon gases (C_2-C_4) was significantly decreased with the introduction of catalyst in particular for the Ca-added catalysts. In addition, it seems that the addition of calcium into catalyst showed a positive effect on hydrogen production. The hydrogen yield increased from 10.4 to 18.2 mmol H_2 g^{-1}sample and hydrogen concentration increased from 35.1 to 52.3 Vol. % after introducing calcium (0.8 Ca) to the Ni-Mg-Al catalyst.

Furthermore, the concentration of CH_4 was significantly reduced from 24.6 to 8.1vol.% by adding Ca to the Ni-Mg-Al catalyst. It seems that introducing Ca promoted methane reforming reaction [36].

Compared to the Ni-Mg-Al catalyst, the surface area of Ca-added Ni-based catalyst was decreased as shown in Table 1. Thus, it is difficult to identify a relationship between textile properties of the catalysts and hydrogen production. It is suggested that Ca-based compound formed in the Ca-Ni-Mg-Al catalyst was responsible for the improved catalytic activity of hydrogen production. It has been reported that the addition of CaO in catalyst system might increase the production of hydrogen by promoting water gas shift reaction as CO_2 was in-situ reacted [37, 38].

The Ni-Mg-Al catalyst with different Ca loadings (10, 30, 50, 80 mol. %), noted as 0.1Ca, 0.3Ca, 0.5Ca and 0.8Ca respectively, was also investigated for biomass gasification. Liquid yield was calculated by the weight of condensed liquid containing tars and un-reacted water divided by the weight of wood sawdust. Due to the amount of injected water could be slight different, the liquid yield was not reliable for interpreting the catalytic activity for biomass gasification. Therefore, gas and hydrogen yield and gas concentration were used to discuss catalytic activities of the developed catalyst. From Table 4, the highest gas yield was observed (74.4 wt. %) for the 0.5Ca catalyst. It is suggested that the highest fraction of small NiO particles, which makes up 54.9% of different Ni based materials (Table 2). It is indicated that the lowest gas yield was produced from the 0.1Ca catalyst.

From Table 4, the gas concentration and hydrogen yield in relation to biomass weight was changed slightly by increasing calcium content in the catalyst. It is suggested that by adding more Ca in the catalyst, the actual available active Ni metals were reduced, as the total amount of the catalyst was the same for each experiment. Therefore, a hydrogen yield associated with nickel mole percentage was calculated and shown in Figure 5. The hydrogen yield obtained in Figure 5 was calculated below (Equation 1):

$$H_2 \text{ yield g/Ni} = H_2 \text{ yield (mmol } H_2 g^{-1} \text{ biomass sample)/ Ni (mol)} \quad (1)$$

The hydrogen yield per mole of nickel increased from 50 g Ni^{-1}(0.8Ca catalyst) to 80g Ni^{-1} when the catalyst changed from the 0.1Ca to the 0.8Ca. It is suggested that CaO played two significant roles during the gasification of biomass. Firstly, it adsorbed carbon dioxide from the generated syngas to increase hydrogen yield by thermodynamically favoring water gas shift reaction. Secondly, CaO might catalytic promote steam reforming of hydrocarbon to form H_2-

rich syngas [18, 19, 39, 40]. In addition, the 0.1Ca catalyst produced much lower hydrogen yield (Table 4) compared with the other Ca-added catalysts. This might be due to the presence of much lower content of small NiO particles in the 0.1Ca catalyst, as shown in Table 2.

In terms of the surface area of the catalyst, as shown in Table 1, the 0.8Ca catalyst has the lowest surface area, which is only 98.8 m^2g^{-1}. However, it showed the highest hydrogen production per unit of Ni. It is therefore indicated that the reactions of biomass catalytic pyrolysis/gasification were dominated by catalytic metal sites of the catalyst, while the diffusion of reactants and products were not key parameters for hydrogen production in this work.

3.3. Characterizations of the reacted catalysts

3.3.1. TPO and XRD analysis

TPO results about the reacted catalyst were presented in Figure 6 and Figure 7. The oxidation peak at around 420 °C was ascribed to amorphous carbons and the TPO peak at around 600 °C was suggested to be filamentous carbon [41]. The peak of mass increase at around 400 °C was associated with the oxidation of Ni produced by the reduction of NiO in the pyrolysis-gasification process [36, 41]. The catalyst without Ca loading exhibited a much lower peak intensity at 400 °C as shown in Figure 6. It is indicated that the content of reducible NiO particles in the Ni-Mg-Al catalyst was very low. It is also suggested that the addition of Ca into Ni-Mg-Al catalyst could significantly enhance the reducibility of the catalyst, thus improving hydrogen production. This is proved from the results in Table 3, where hydrogen yield was increased with the addition of Ca.

Due to the large intensity of Ni oxidation for the reacted Ca-added Ni-Mg-Al catalysts in the TPO analysis, an overlap between the weight increase (Ni oxidation) and the weight loss (carbon oxidation) might be existed. Therefore, TPO-FTIR had been conducted to obtain clear information about the oxidation of carbon formed on the reacted catalysts.

As shown in Figure 8, with the increase of calcium loading from 0.1Ca to 0.5Ca, the amount of oxidized carbons was increased. In addition, a big oxidation peak was observed at around 400 °C indicating that more amorphous carbons was generated with the 0.5Ca catalyst. This phenomenon is attributed to that the 0.5Ca catalyst contained the largest amount of small NiO particles (54.9%) as shown in Table 2. Small NiO particles are reactive for carbon formation

8

in thermal cracking reactions, which is consistent with the highest gas yield obtained by the 0.5Ca catalyst (Table 4). In addition, the 0.5Ca catalyst also generated the largest amount of filamentous carbon, corresponding to the highest oxidation near 650 °C in the TPO analysis (Figure 7) [42, 43]. Therefore, although the addition of Ca can increase hydrogen production from biomass gasification, the deactivation of catalyst as ascribed to the formation of coke on the surface still needs to be further investigated.

However, with the further increase of calcium loading to 0.8Ca, the intensity of carbon oxidation is decreased due to the presence of $NiAl_2O_4$, which performed a positive effect on decreasing the coke deposition on the surface of reacted catalyst [44, 45].

3.3.2. SEM and TEM analysis

The surface morphology of the experimented catalysts obtained by SEM analysis is shown in Figure 9. It can be seen that some filamentous carbons were generated on the experimented catalysts. Furthermore, compared to the reacted Ni-Ca-Mg-Al catalyst, an obvious formation of filamentous carbon generated by the reacted Ni-Ca-Al and Ni-Mg-Al catalysts. In addition, the reacted 0.5Ca catalyst shows the most obvious coke deposition, which is consistent with the data obtained the TPO analysis (Figure 3.8).

Selected TEM results of the reacted 0.1Ca, 0.5Ca and 0.8Ca catalysts were demonstrated in Figure 9. Ni particles were observed for all the reacted catalysts. It is difficult to observe filamentous carbons since the amount of carbon formed on the surface of the reacted catalyst was very small. As shown in Figure 10, the particle size for the reacted 0.8Ca catalyst is around 35 nm, which is similar to the fresh 0.8 catalyst (28nm in Table 1).

Conclusions

In this work, cost-effective Ca added Ni-based catalysts were developed and studied for producing hydrogen from steam biomass gasification using a fixed-bed reactor. The relationship between Ca addition and the performance of catalyst in relation to the yield of hydrogen and metal sintering and coke formation on reacted catalyst was studied. The results showed that incorporating Ca into the Ni-Mg-Al catalyst was effective for enhancing hydrogen production sequentially reducing the cost of catalyst. For example, the yield of hydrogen was increased from 10.4 to 18.2 mmol g^{-1} sample, when Ca was introduced in to the Ni-Mg-Al catalyst. This is attributed to enhanced adsorption of CO_2 using CaO and thus promoted the

water gas shift reaction in the gasification process. TPO-FTIR analysis of the experimented catalysts showed that the 0.5 Ca catalyst had the highest amount of coke formation, in particular, most of the deposited carbons were amorphous which could deactivate the catalyst seriously. It is therefore concluded that the addition of cost-effective Ca could enhance the yield of hydrogen from biomass. However, the concentration of Ca in the catalyst needs to be controlled to mitigate the formation of coke on the used catalyst.

Acknowledgement

References

[1] M. Ball, M. Wietschel, The future of hydrogen - opportunities and challenges, International Journal of Hydrogen Energy, 34 (2009) 615-627.

[2] M. Barati, M. Babatabar, A. Tavasoli, A.K. Dalai, U. Das, Hydrogen production via supercritical water gasification of bagasse using unpromoted and zinc promoted Ru/γ-Al2O3 nanocatalysts, Fuel Processing Technology, 123 (2014) 140-148.

[3] J. Nishikawa, T. Miyazawa, K. Nakamura, M. Asadullah, K. Kunimori, K. Tomishige, Promoting effect of Pt addition to Ni/CeO2/Al2O3 catalyst for steam gasification of biomass, Catalysis Communications, 9 (2008) 195-201.

[4] C. Wu, P.T. Williams, Hydrogen production by steam gasification of polypropylene with various nickel catalysts, Applied Catalysis B: Environmental, 87 (2009) 152-161.

[5] C. Wu, Z. Wang, J. Huang, P.T. Williams, Pyrolysis/gasification of cellulose, hemicellulose and lignin for hydrogen production in the presence of various nickel-based catalysts, Fuel, 106 (2013) 697-706.

[6] Y. Richardson, J. Blin, G. Volle, J. Motuzas, A. Julbe, In situ generation of Ni metal nanoparticles as catalyst for H2-rich syngas production from biomass gasification, Applied Catalysis A: General, 382 (2010) 220-230.

[7] X. Cai, X. Dong, W. Lin, Effect of CeO2 on the catalytic performance of Ni/Al2O3 for autothermal reforming of methane, Journal of Natural Gas Chemistry, 17 (2008) 98-102.

[8] I.N. Buffoni, F. Pompeo, G.F. Santori, N.N. Nichio, Nickel catalysts applied in steam reforming of glycerol for hydrogen production, Catalysis Communications, 10 (2009) 1656-1660.

[9] K.-S. Hwang, H.Y. Zhu, G.Q. Lu, New nickel catalysts supported on highly porous alumina intercalated laponite for methane reforming with CO2, Catalysis Today, 68 (2001) 183-190.

[10] K. Takehira, T. Shishido, P. Wang, T. Kosaka, K. Takaki, Autothermal reforming of CH4 over supported Ni catalysts prepared from Mg–Al hydrotalcite-like anionic clay, Journal of Catalysis, 221 (2004) 43-54.

[11] S. Sengupta, G. Deo, Modifying alumina with CaO or MgO in supported Ni and Ni–Co catalysts and its effect on dry reforming of CH4, Journal of CO2 Utilization, 10 (2015) 67-77.

[12] J. Zhang, H. Wang, A.K. Dalai, Effects of metal content on activity and stability of Ni-Co bimetallic catalysts for CO2 reforming of CH4, Applied Catalysis A: General, 339 (2008) 121-129.

[13] W.K. Jóźwiak, M. Nowosielska, J. Rynkowski, Reforming of methane with carbon dioxide over supported bimetallic catalysts containing Ni and noble metal: I. Characterization and activity of SiO2 supported Ni–Rh catalysts, Applied Catalysis A: General, 280 (2005) 233-244.

[14] A.A. Al-Musa, Z.S. Ioakeimidis, M.S. Al-Saleh, A. Al-Zahrany, G.E. Marnellos, M. Konsolakis, Steam reforming of iso-octane toward hydrogen production over mono- and bi-metallic Cu–Co/CeO2 catalysts: Structure-activity correlations, International Journal of Hydrogen Energy, 39 (2014) 19541-19554.

[15] V.R. Choudhary, B.S. Uphade, A.S. Mamman, Large enhancement in methane-to-syngas conversion activity of supported Ni catalysts due to precoating of catalyst supports with MgO, CaO or rare-earth oxide, Catalysis Letters, 32 (1995) 387-390.

[16] A.A. Lemonidou, I.A. Vasalos, Carbon dioxide reforming of methane over 5 wt.% Ni/CaO-Al2O3 catalyst, Applied Catalysis A: General, 228 (2002) 227-235.

[17] M.C.J. Bradford, M.A. Vannice, CO2 Reforming of CH4, Catalysis Reviews, 41 (1999) 1-42.

[18] Z. Hou, O. Yokota, T. Tanaka, T. Yashima, Characterization of Ca-promoted Ni/α-Al2O3 catalyst for CH4 reforming with CO2, Applied Catalysis A: General, 253 (2003) 381-387.

[19] K.F.M. Elias, A.F. Lucrédio, E.M. Assaf, Effect of CaO addition on acid properties of Ni–Ca/Al2O3 catalysts applied to ethanol steam reforming, International Journal of Hydrogen Energy, 38 (2013) 4407-4417.

[20] C.K.S. Choong, Z. Zhong, L. Huang, Z. Wang, T.P. Ang, A. Borgna, J. Lin, L. Hong, L. Chen, Effect of calcium addition on catalytic ethanol steam reforming of Ni/Al2O3: I. Catalytic stability, electronic properties and coking mechanism, Applied Catalysis A: General, 407 (2011) 145-154.

[21] L. Wei, H. Yang, B. Li, X. Wei, L. Chen, J. Shao, H. Chen, Absorption-enhanced steam gasification of biomass for hydrogen production: Effect of calcium oxide addition on steam gasification of pyrolytic volatiles, International Journal of Hydrogen Energy, 39 (2014) 15416-15423.

[22] M. Broda, A.M. Kierzkowska, D. Baudouin, Q. Imtiaz, C. Copéret, C.R. Müller, Sorbent-Enhanced Methane Reforming over a Ni–Ca-Based, Bifunctional Catalyst Sorbent, ACS Catalysis, 2 (2012) 1635-1646.

[23] K.Y. Koo, J.H. Lee, U.H. Jung, S.H. Kim, W.L. Yoon, Combined H2O and CO2 reforming of coke oven gas over Ca-promoted Ni/MgAl2O4 catalyst for direct reduced iron production, Fuel, 153 (2015) 303-309.

[24] Z.L. Zhang, X.E. Verykios, Carbon dioxide reforming of methane to synthesis gas over supported Ni catalysts, Catalysis Today, 21 (1994) 589-595.

[25] F. Chen, C. Wu, L. Dong, A. Vassallo, P.T. Williams, J. Huang, Characteristics and catalytic properties of Ni/CaAlOx catalyst for hydrogen-enriched syngas production from pyrolysis-steam reforming of biomass sawdust, Applied Catalysis B: Environmental, 183 (2016) 168-175.

[26] O. Clause, M. Gazzano, F. Trifiro, A. Vaccari, L. Zatorski, Preparation and thermal reactivity of nickel/chromium and nickel/aluminium hydrotalcite-type precursors, Applied Catalysis, 73 (1991) 217-236.

[27] C. Wu, P.T. Williams, Investigation of Ni-Al, Ni-Mg-Al and Ni-Cu-Al catalyst for hydrogen production from pyrolysis–gasification of polypropylene, Applied Catalysis B: Environmental, 90 (2009) 147-156.

[28] S. Li, L. Guo, C. Zhu, Y. Lu, Co-precipitated Ni–Mg–Al catalysts for hydrogen production by supercritical water gasification of glucose, International Journal of Hydrogen Energy, 38 (2013) 9688-9700.

[29] M. Abdollahifar, M. Haghighi, A.A. Babaluo, Syngas production via dry reforming of methane over Ni/Al2O3–MgO nanocatalyst synthesized using ultrasound energy, Journal of Industrial and Engineering Chemistry, 20 (2014) 1845-1851.

[30] L. Garcia, A. Benedicto, E. Romeo, M.L. Salvador, J. Arauzo, R. Bilbao, Hydrogen Production by Steam Gasification of Biomass Using Ni−Al Coprecipitated Catalysts Promoted with Magnesium, Energy & Fuels, 16 (2002) 1222-1230.

[31] A.M. Diskin, R.H. Cunningham, R.M. Ormerod, The oxidative chemistry of methane over supported nickel catalysts, Catalysis Today, 46 (1998) 147-154.

[32] B. Roy, K. Loganathan, H.N. Pham, A.K. Datye, C.A. Leclerc, Surface modification of solution combustion synthesized Ni/Al2O3 catalyst for aqueous-phase reforming of ethanol, International Journal of Hydrogen Energy, 35 (2010) 11700-11708.

[33] W.S. Dong, H.S. Roh, K.W. Jun, S.E. Park, Y.S. Oh, Methane reforming over Ni/Ce-ZrO2 catalysts: Effect of nickel content, Applied Catalysis A: General, 226 (2002) 63-72.

[34] R. Ran, G. Xiong, W. Yang, An in-situ modified sol-gel process for monolith catalyst preparation used in the partial oxidation of methane, Journal of Materials Chemistry, 12 (2002) 1854-1859.

[35] I.O. Cruz, N.F.P. Ribeiro, D.A.G. Aranda, M.M.V.M. Souza, Hydrogen production by aqueous-phase reforming of ethanol over nickel catalysts prepared from hydrotalcite precursors, Catalysis Communications, 9 (2008) 2606-2611.

[36] S. Kumagai, J. Alvarez, P.H. Blanco, C. Wu, T. Yoshioka, M. Olazar, P.T. Williams, Novel Ni–Mg–Al–Ca catalyst for enhanced hydrogen production for the pyrolysis–gasification of a biomass/plastic mixture, Journal of Analytical and Applied Pyrolysis.

[37] M.A. Nahil, X. Wang, C. Wu, H. Yang, H. Chen, P.T. Williams, Novel bi-functional Ni-Mg-Al-CaO catalyst for catalytic gasification of biomass for hydrogen production with in situ CO_2 adsorption, RSC Advances, 3 (2013) 5583-5590.

[38] C. Wang, B. Dou, B. Jiang, Y. Song, B. Du, C. Zhang, K. Wang, H. Chen, Y. Xu, Sorption-enhanced steam reforming of glycerol on Ni-based multifunctional catalysts, International Journal of Hydrogen Energy, 40 (2015) 7037-7044.

[39] J.-H. Kuo, M.-Y. Wey, W.-C. Chen, Woody waste air gasification in fluidized bed with Ca- and Mg-modified bed materials and additives, Applied Thermal Engineering, 53 (2013) 42-48.

[40] C.K.S. Choong, L. Huang, Z. Zhong, J. Lin, L. Hong, L. Chen, Effect of calcium addition on catalytic ethanol steam reforming of Ni/Al2O3: II. Acidity/basicity, water adsorption and catalytic activity, Applied Catalysis A: General, 407 (2011) 155-162.

[41] C.S. Wu, Y. Sun, M. Vestergaard, J. Christensen, R.B. Ness, C.L. Haggerty, J. Olsen, Preeclampsia and risk for epilepsy in offspring, Obstetrical and Gynecological Survey, 64 (2009) 152-153.

[42] I.F. Elbaba, C. Wu, P.T. Williams, Hydrogen production from the pyrolysis–gasification of waste tyres with a nickel/cerium catalyst, International Journal of Hydrogen Energy, 36 (2011) 6628-6637.

[43] C. Wu, P.T. Williams, Ni/CeO2/ZSM-5 catalysts for the production of hydrogen from the pyrolysis–gasification of polypropylene, International Journal of Hydrogen Energy, 34 (2009) 6242-6252.

[44] Y.-g. Chen, J. Ren, Conversion of methane and carbon dioxide into synthesis gas over alumina-supported nickel catalysts. Effect of Ni-Al2O3 interactions, Catalysis Letters, 29 (1994) 39-48.

[45] H. Muroyama, R. Nakase, T. Matsui, K. Eguchi, Ethanol steam reforming over Ni-based spinel oxide, International Journal of Hydrogen Energy, 35 (2010) 1575-1581.

Table 1 Textural characteristic of fresh catalysts

Sample (mole ratio)	Surface area (m^2g^{-1})	Particle Size (nm)
Ca Ni Mg Al (1:2:2:1)	79.48	17.98
Ni Mg Al(2:2:1) (no Ca)	126.29	8.80
Ca Ni Al (1:2:1) (no Mg)	96.54	17.32
0.1 Ca Ni Mg Al (1:1:1)	153.27	19.85
0.3 Ca Ni Mg Al (1:1:1)	145.16	20.63
0.5 Ca Ni Mg Al (1:1:1)	138.31	21.27
0.8 Ca Ni Mg Al (1:1:1)	98.88	27.53

Particle size obtained from XRD data calculated based on the Scherrer's formula.

Table 2 Contents of Ni-based materials based on TPR analysis

Sample	Bulk NiO ratio (mol%)	Small NiO ratio (mol%)	NiAl$_2$O$_4$ ratio (mol%)
0.1Ca	6.4	6.37	87.2
0.3Ca	8.3	26.2	65.5
0.5Ca	10.8	54.9	34.2
0.8Ca	22.4	18.1	59.4

Table 3 Mass balance and gas compositions from gasification of biomass

Catalyst bed	Blank	Ni-Ca-Mg-Al (1:1:1:1)	Ni-Mg-Al (1:1:1)
Gas/wood (wt. %)	53.7	55.8	53.3
Liquid yield (wt. %)	82.3	77.9	83.7
Mass balance (wt. %)	97.55	94.03	97.52
H_2 yield (mmol H_2 g^{-1}sample)	6.0	18.2	10.4
Gas composition (Vol.%, N_2 free)			
CO	29.7	23.0	25.3
H_2	23.2	52.3	35.1
CO_2	14.1	16.2	12.3
CH_4	29.4	8.1	24.6
C_2-C_4	3.5	0.4	2.6

Table 4 Mass balance and gas compositions from gasification of biomass of with different calcium ratio

Catalyst bed	0.8Ca	0.5Ca	0.3Ca	0.1Ca
Gas/wood (wt. %)	67.6	74.4	65.9	57.4
Liquid yield (wt. %)	75.9	82.2	77.4	81.4
Mass balance (wt. %)	92.19	99.34	96.02	97.85
H_2 yield (mmol H_2 g^{-1} sample)	20.4	20.6	21.4	16.3
Gas composition (Vol.%, N_2 free)				
CO	24.0	22.4	22.5	21.1
H_2	49.6	49.0	53.3	47.3
CO_2	15.7	20.5	18.2	16.2
CH_4	9.9	7.7	5.5	14.3
C_2-C_4	0.9	0.3	0.5	1.0
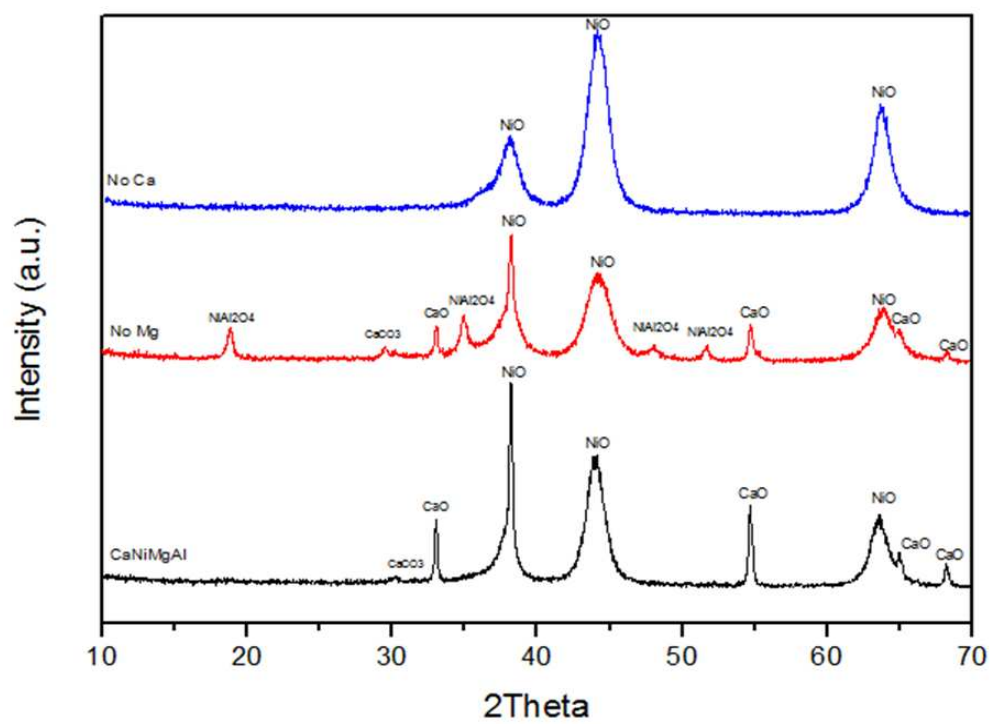
Figure 1 XRD analysis of the fresh catalyst
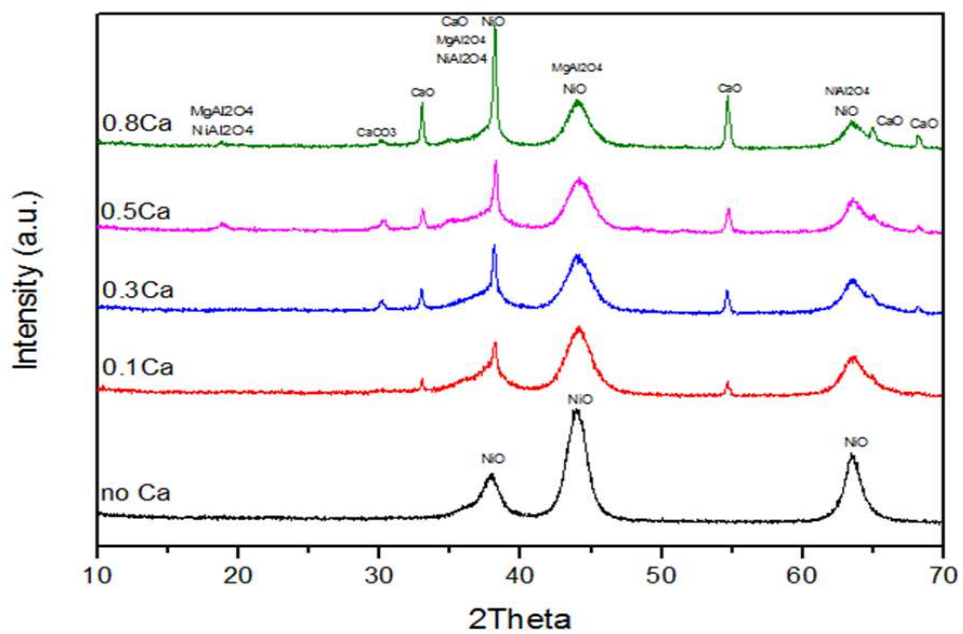
Figure 2 XRD analysis of the fresh Ni-Ca-Mg-Al catalyst with different calcium ratios
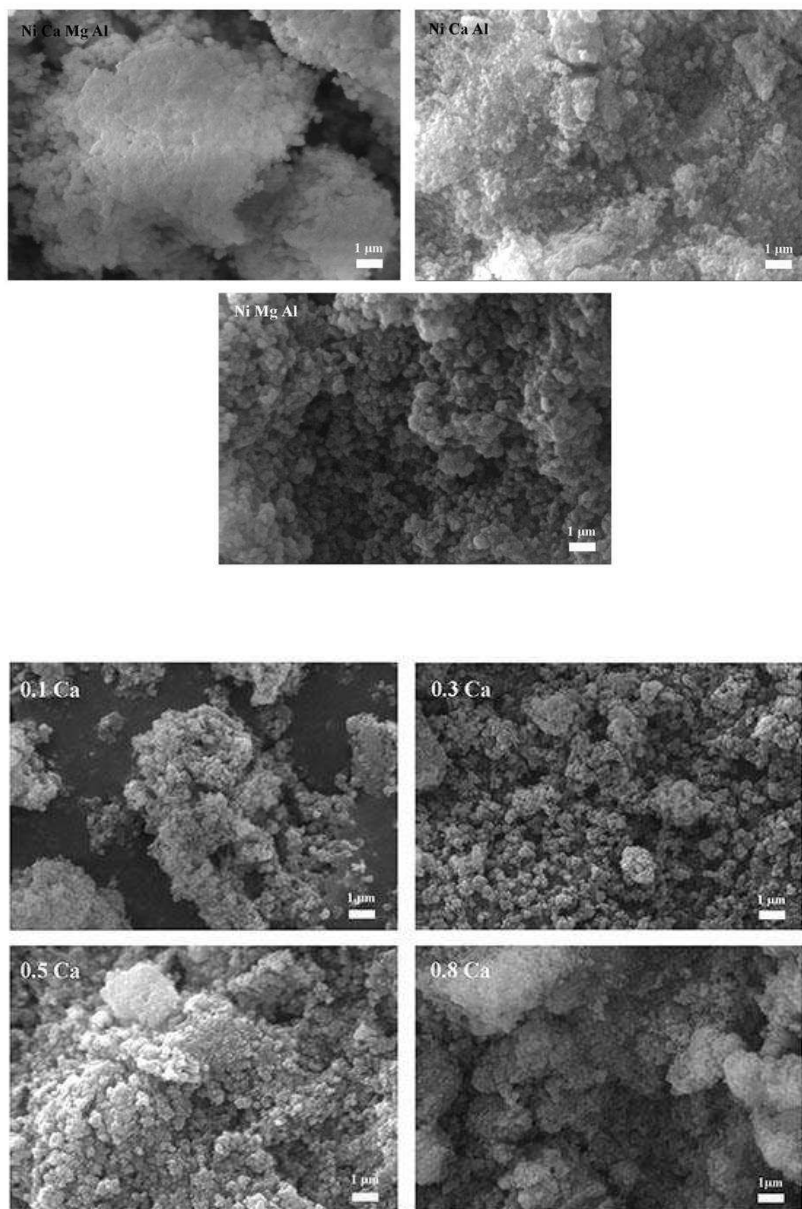
Figure 3 SEM images of fresh Ni-Ca-Mg-Al catalysts
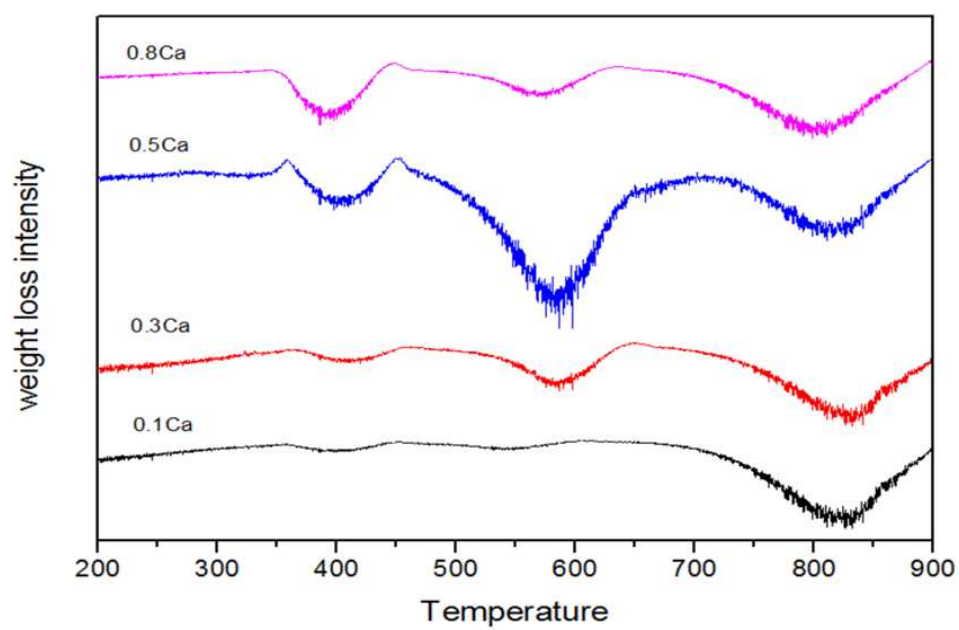
Figure 4 TPR analysis of fresh Ni-Ca-Mg-Al catalysts
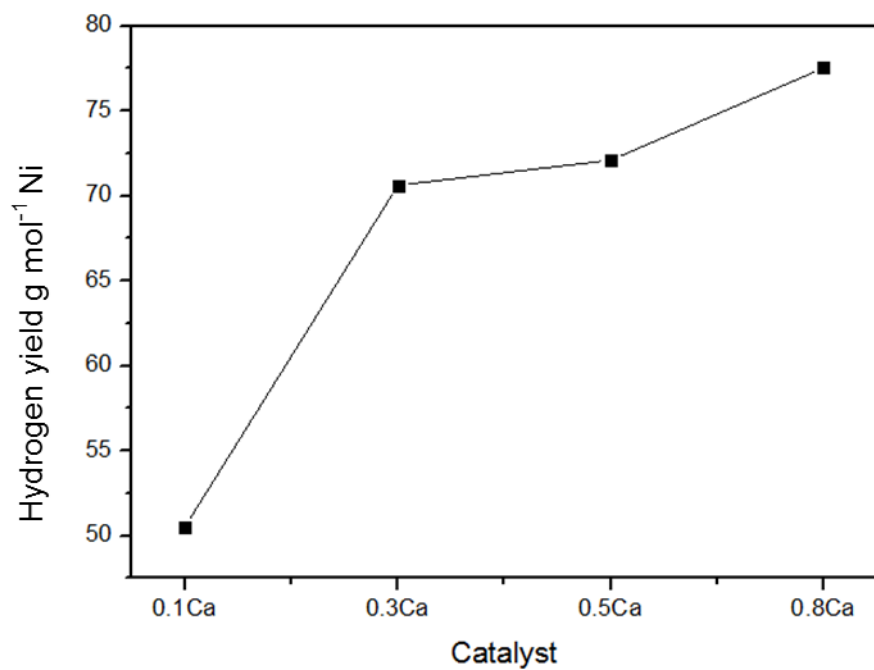
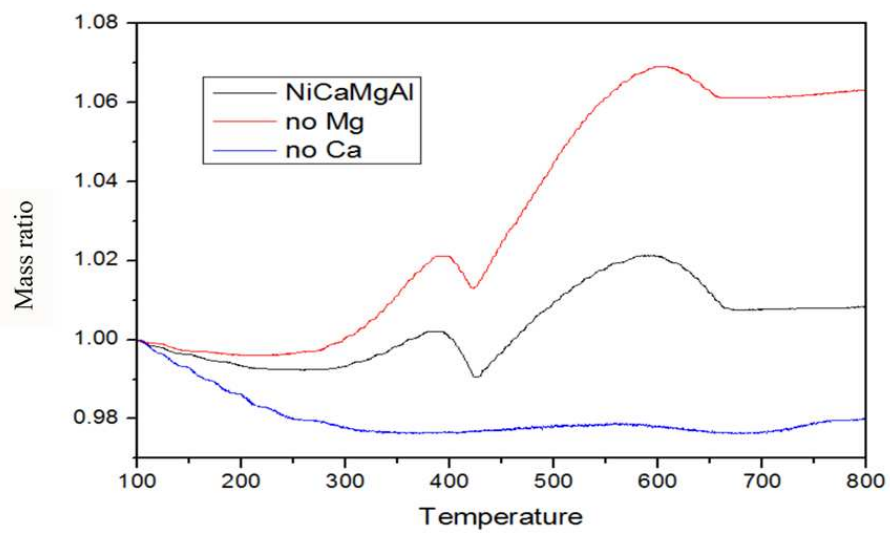Figure 5 H$_2$ yield change with different Calcium concentration catalysts
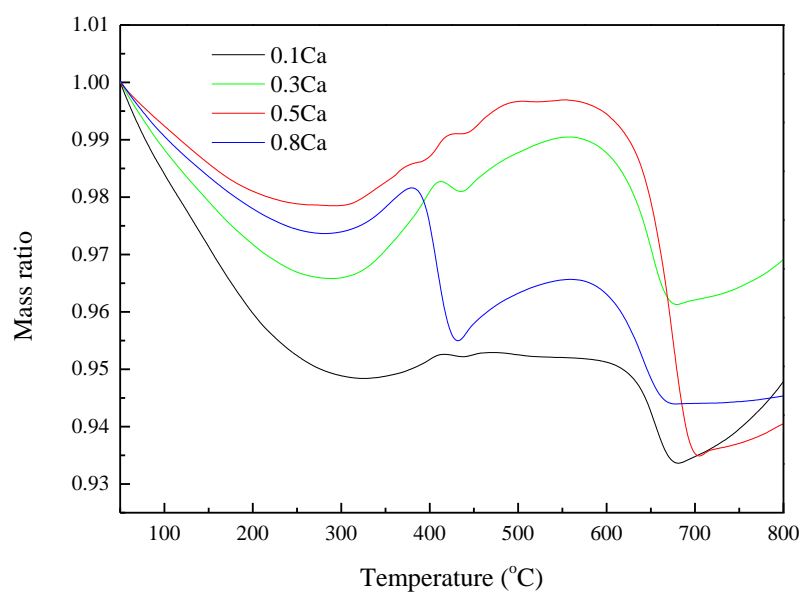
Figure 6 TPO analysis of the catalyst

Figure 7 TPO analysis results of the reacted catalysts with different Ca ratios
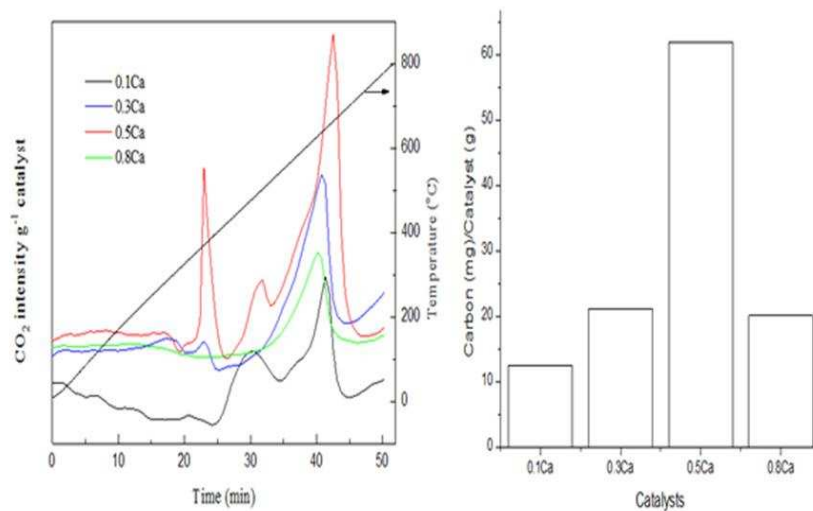
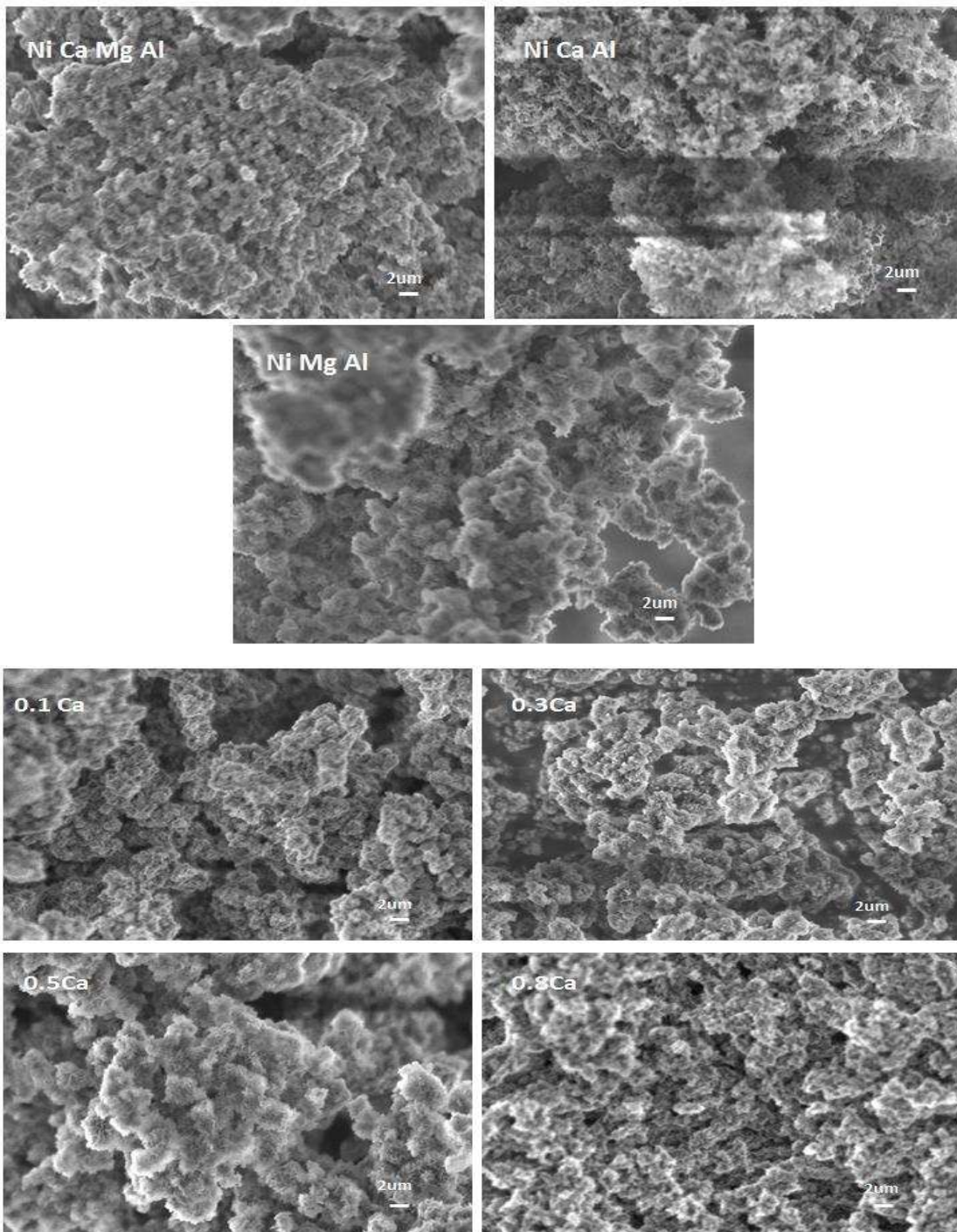Figure 8 CO$_2$-FTIR results during the TPO experiment
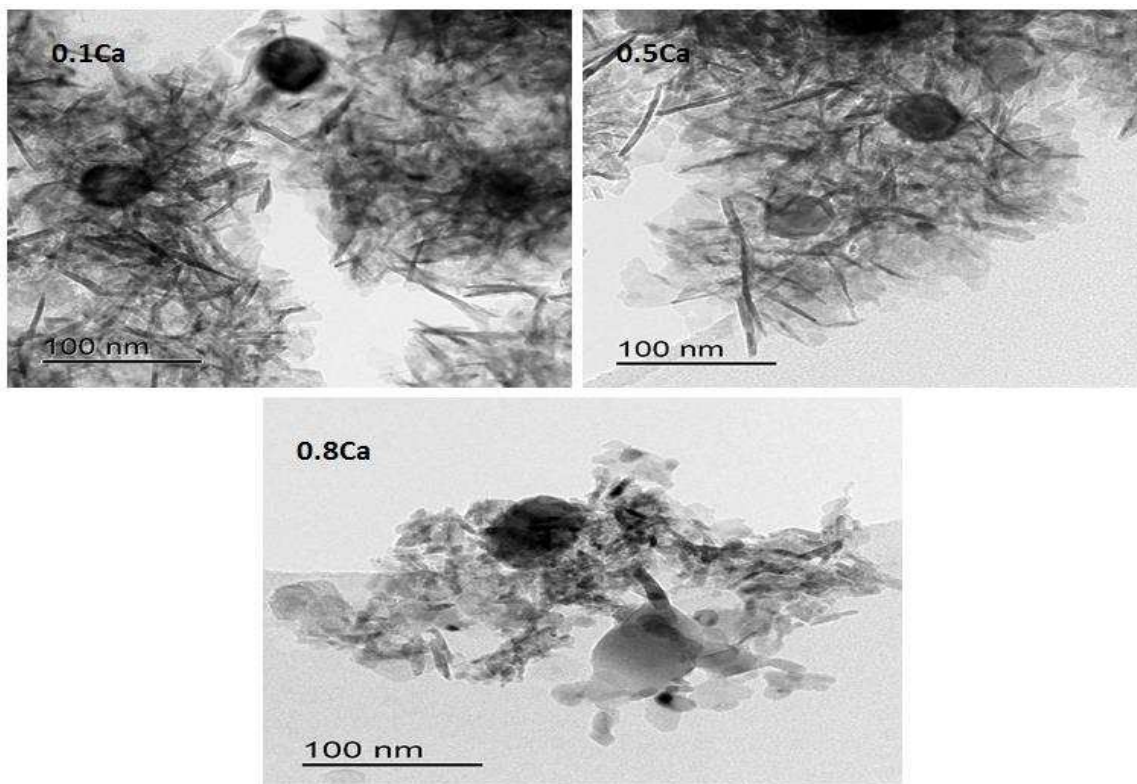
Figure 9 SEM images of reacted Ni-Ca-Mg-Al catalysts

Figure 10 Typical TEM images of reacted catalysts